Chirality in Magnetic Multilayers Probed by the Symmetry and the Amplitude of Dichroism in X-Ray Resonant Magnetic Scattering

Jean-Yves Chauleau,[1,2,*] William Legrand,[2] Nicolas Reyren,[2] Davide Maccariello,[2] Sophie Collin,[2] Horia Popescu,[1] Karim Bouzehouane,[2] Vincent Cros,[2,†] Nicolas Jaouen,[1] and Albert Fert[2]
[1]*Synchrotron SOLEIL, L'Orme des Merisiers, 91192 Gif-sur-Yvette, France*
[2]*Unité Mixte de Physique, CNRS, Thales, Université Paris-Sud, Université Paris-Saclay, 91767 Palaiseau, France*

(Received 22 September 2017; published 18 January 2018)

Chirality in condensed matter has recently become a topic of the utmost importance because of its significant role in the understanding and mastering of a large variety of new fundamental physical mechanisms. Versatile experimental approaches, capable to reveal easily the exact winding of order parameters, are therefore essential. Here we report x-ray resonant magnetic scattering as a straightforward tool to reveal directly the properties of chiral magnetic systems. We show that it can straightforwardly and unambiguously determine the main characteristics of chiral magnetic distributions: i.e., its chiral nature, the quantitative winding sense (clockwise or counterclockwise), and its type, i.e., Néel [cycloidal] or Bloch [helical]. This method is model independent, does not require *a priori* knowledge of the magnetic parameters, and can be applied to any system with magnetic domains ranging from a few nanometers (wavelength limited) to several microns. By using prototypical multilayers with tailored magnetic chiralities driven by spin-orbit-related effects at Co|Pt interfaces, we illustrate the strength of this method.

DOI: 10.1103/PhysRevLett.120.037202

Chirality is central to understanding many fundamental mechanisms in various domains of physics and chemistry. In condensed matter, a large variety of physical phenomena hinge upon the emergence of these complex chiral windings of order parameters, their observation, and subsequently their control, especially in magnetism and spintronics at the nanoscale. The ability to probe the nature of these chiral magnetic textures has now become a crucial element of modern magnetism and is therefore essential to gain a deeper understanding of these mechanisms. Magnetic textures with a cycloidal configuration of the magnetization, such as Néel domain walls (DWs), are stabilized in ultrathin magnetic films (one or a few atomic layers) on heavy metal substrates [1]. It was realized that these magnetic textures are stabilized by an interfacial Dzyaloshinskii-Moriya (DM) interaction [2,3] ($\sum_{ij} \boldsymbol{D}_{ij} \cdot \boldsymbol{S}_i \times \boldsymbol{S}_j$, with $\boldsymbol{S}_i$ and $\boldsymbol{S}_j$ two neighboring spins), which is the antisymmetric analog of the Heisenberg interaction favoring a curling magnetization texture around the DM vector $\boldsymbol{D}$. The DM interaction requires spin-orbit coupling and broken inversion symmetry, found either in specific crystalline structures, such as B20 materials [4], or at film interfaces [5,6]. One important requirement is therefore a full and unambiguous access to the chiral nature of magnetization textures and hence a direct measurement to the DM vector. Different methods have already been utilized to access the texture of the DWs or Skyrmions such as spin-polarized STM [1,7], scanning nitrogen-vacancy magnetometry [8,9], spin-polarized low-energy electron microscopy [10], or Lorentz transmission electron microscopy [11]. On the other hand, the DM interaction has also been probed by spin wave spectroscopy techniques such as Brillouin light scattering [12] or time-resolved Kerr microscopy [13]. Once the type of winding is determined, the chirality [clockwise (CW) or counterclockwise (CCW)] of the Néel textures is usually indirectly deduced, for example, from DW dynamics and micromagnetic comparison [14].

In this Letter, we demonstrate that x-ray resonant magnetic scattering (XRMS) experiments [see a schematic description in Fig. 1(a)] allow us to reveal the actual magnetic textures existing in ultrathin magnetic multilayers with perpendicular anisotropy and a large interfacial DM interaction. Importantly, this determination is straightforward and does not require any assumptions or careful comparison to parameter-dependent micromagnetic simulations. Already in 1999, Dürr *et al.* [15] showed the ability of XRMS experiments to reveal the chiral nature of closure magnetic domains at the topmost surface of a 40-nm-thick FePd layer. Here we prove by a thorough analysis that the magnetic asymmetry (dichroism renormalized by the intensities) in XMRS enables us to directly identify not only the direction (like in Ref. [15]) but also the sense of the magnetic winding and therefore of the actual sign of DM interaction. This information has a far-reaching impact, in particular for spin-orbitronics and spin-orbit torque (SOT) studies. Indeed, SOT is a very promising approach to move efficiently domain walls [16] and magnetic Skyrmions along magnetic racetracks [17] and shows therefore a great potential for future spintronic devices. Yet, the detailed texture of the domain walls plays a major role in their motion [16]. Indeed, the DW high speed is related to its nature (Néel or Bloch), while its direction of motion depends on its chirality [18–20]. Another important impact of the DM

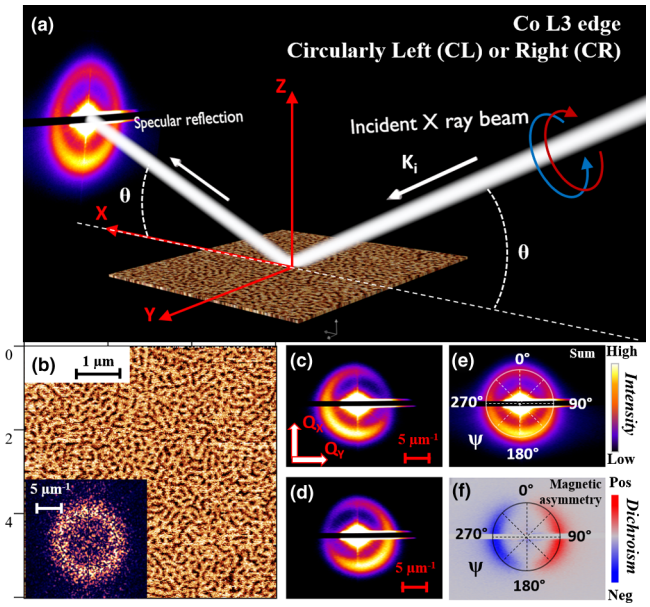

FIG. 1. (a) XRMS measurement principle and experimental configuration. (b) $6 \times 6\ \mu m^2$ MFM phase image showing the out-of-plane magnetic contrast of the $[Ir(1)|Co(0.6)|Pt(1)] \times 5$ multilayer with its corresponding FFT pattern (inset) evidencing a 180 ± 30 nm period disordered magnetic stripe pattern. Corresponding diffracted patterns for a CL (c) and CR (d) polarized incident x-ray beam. (e) Resulting sum image of the diffracted pattern (CL + CR), confirming that the diffraction corresponds to the magnetic domains observed by MFM. (f) Normalized difference image (CL-CR/CL + CR) evidencing a pronounced magnetic asymmetry. Note that the straight black area crossing the diffraction ring is the shadow of a beamstop used to block the specular reflection.

interaction that has been largely overlooked (see, e.g., [21,22]) is its role on the performances in spintronics applications already using ultrathin magnetic multilayers with perpendicular magnetic anisotropy such as MRAM or detectors. All of these makes essential the need to probe the consequences of interfacial DM on actual magnetic textures.

XMRS presents several advantages that might soon turn it to a standard way to characterize and quantify the DM interaction, even though it requires access to a synchrotron facility. First, XMRS is a nonperturbative technique contrary to the approach based on magnetic domain analysis through magnetic force microscopy (MFM) imaging or domain wall motion. Second, such a study is applicable not only to metallic chiral magnets but can be extended to the substantial number of insulating magnetic systems with element specificity, i.e., the ability to distinguish between the different elements of a sample by tuning the photon energy accordingly. Third, this experiment is based on the scattering on magnetic domains and DWs, making sample patterning not required. Then, XRMS is sensitive to thicknesses of less than a few nanometers of total magnetic materials (either in a single film or in multilayers) that conveniently can be buried below a few nanometers of materials (e.g., capping). Finally, XMRS experiments might easily be extended in the near future to time-resolved experiments using a synchrotron [23] or free electron laser [24], which should open new horizons to the exploration of the dynamics of magnetic chirality.

In this study, we perform XRMS experiments using circularly polarized x rays on prototypical Co|Pt-based perpendicularly magnetized multilayers which have proven to be a system of choice for the emergence of homochiral magnetic distributions and are consequently also prototypical for SOT applications [25,26]. Our magnetic multilayers have been prepared using magnetron sputtering on thermally oxidized silicon substrates (see [27] for details). Two types of multilayers composed of fivefold repetition of a trilayer are considered: $\|[Pt(1\ nm)|Co(0.8\ nm)|Ir(1\ nm)] \times 5$ and its reversed-stacking counterpart $\|[Ir(1\ nm)|Co(t)|Pt(1\ nm)] \times 5$. The symbol "$\|$" stands for the substrate and the 10-nm-thick Pt buffer. To avoid oxidation, a 3-nm-thick Pt capping is deposited on top of the multilayers. In these samples, we measure a saturation magnetization $M_S \approx 1$ MA/m and a large effective out-of-plane anisotropy $K_{\mathrm{eff}} \approx 0.1\ \mathrm{MJ/m^3}$. According to our previous studies on these systems [27], the mean DM magnitude (arising mainly from the Pt|Co interfaces but with a small additive effect from Co|Ir interfaces) is about $2\ \mathrm{mJ/m^2}$. Such a DM magnitude is large enough to impose Néel DW texture [19,28], with a CCW sense of rotation in the case of a thin Co layer deposited on top of Pt, and conversely a CW Néel DW in the case of Pt is deposited on Co. Before running the XRMS experiments, magnetic domain configurations have been imaged at room temperature using MFM after a demagnetization process using an out-of-plane field. In Fig. 1(b), we display a characteristic randomly disordered magnetic stripe patterns with a mean period of about 180 ± 30 nm [see the FFT of the MFM image in the inset in Fig. 1(b)]. For the reported experiment, magnetic domains with a reasonable degree of periodicity are required for the experiment to be carried out in an optimum way. Note that this will not be a restriction anymore in the next generation of light sources, as they will allow us to use coherent magnetic scattering to recover the local magnetic information, too.

We have performed our XRMS experiments on the two types of multilayer stacking at the SEXTANTS beam line [29] of the SOLEIL synchrotron in France. They have been conducted in reflectivity conditions for circularly left (CL) and right (CR) incident x-ray beam polarizations at the Co L_3 edge (photon energy = 778.2 eV) using the RESOXS diffractometer [30]. The diffracted x rays are collected on a Peltier-cooled square CCD detector covering 6.1° at the working distance of this study. Typical diffracted patterns of the domain structure are displayed in Figs. 1(c)–1(e). All the images have been geometrically corrected along the Q_x direction in order to account for the projection related to the photon incidence angle θ of 18.5° in this case. Note that this

particular angle corresponds to the first multilayer Bragg peak for this particular multilayer. Similarly, for the studied samples, we have carried out the measurements at their first multilayer Bragg peaks so as to ensure comparable scattering conditions. As shown in Fig. 1(e), the sum of the images obtained with CR [Fig. 1(c)] and CL [Fig. 1(d)] polarized light gives rise to a clear ring-shaped diffraction pattern around the specular beam (blocked by a beamstop to avoid saturation of the CCD) in the reciprocal plane (Q_x,Q_y). The ring radius, labeled as q_p, indicates the in-plane isotropy of the domain sizes with a typical periodicity in real space $p=2\pi/q_p$. The domain size $p/2$ of 90 ± 9 nm agrees with the one determined by MFM [see Fig. 1(b)], as the Fourier transform of the MFM image can be directly compared to the XRMS sum image. The magnetic asymmetry, also known as circular dichroism of the scattering signal divided by the sum of scattered intensities, is defined as $(I_{\mathrm{CL}}-I_{\mathrm{CR}})/(I_{\mathrm{CL}}+I_{\mathrm{CR}})$, where I_{CL} and I_{CR} are the intensities collected by the camera for CL and CR polarizations, respectively. A nonhomogeneous intensity of the "sum" image along the Q_x direction can be also noticed. This is due to the difference of angles of the outgoing beams in the small angle scattering geometry. Normalizing by the "sum" allows us to get rid of such a global vertical intensity variation in the magnetic asymmetry. The colored map of the diffracted magnetic asymmetry in Fig. 1(f) displays two lobes, one blue and one red, indicating an opposite dichroism sign. The amplitude of the dichroism is rather large, typically 10% of the sum signal, and for sure sufficient to univocally reveal the nature of the DW texture as explained hereafter.

Indeed, XRMS has been recently used by Zhang, van der Laan, and Hesjedal [31] to characterize the topology of magnetic bulk compounds hosting Skyrmions. In this case, the winding number of Skyrmion lattices in Cu_2OSeO_3 is determined through the analysis of the symmetry of the scattering signal. In our work, by leveraging the dichroism in the XRMS scattering signal observed with circularly polarized light, we demonstrate how it provides a simple and straightforward novel approach to identify the nature of DW texture, i.e., its character (Néel or Bloch) and the magnetic chirality. We believe that these results are of high importance given the considerable recent interest for this type of magnetic multilayers with a large interfacial DM interaction leading to promising applications for a new generation of spin-orbitronic devices [32].

In order to precisely analyze the dichroism in XRMS, we use the following expression of the diffracted intensity $I(\boldsymbol{Q})$ for a scattering vector $\boldsymbol{Q}=\boldsymbol{k}_f-\boldsymbol{k}_i$ in the kinematical approximation:

$$I(\boldsymbol{Q}) \propto \left|\sum\nolimits_n f_n \exp(i\boldsymbol{Q}\cdot\boldsymbol{r}_n)\right|^2,$$

where f_n is the resonant scattering amplitude of a single ion at the r_n position in the electron-dipole approximation. In case this ion carries a magnetic moment $\boldsymbol{m}_n$, different contributions to this scattering amplitude can be distinguished at resonance [33–35] $f_n=f_0+f_m^1+f_m^2$, where f_0 is the anomalous charge scattering amplitude and f_m^1 and f_m^2 are the magnetic resonant scattering amplitudes:

$$f_m^1 \propto -i(\hat{\epsilon}\times\hat{\epsilon}')\cdot\boldsymbol{m}_n,$$
$$f_m^2 \propto (\hat{\epsilon}'\cdot\boldsymbol{m}_n)(\hat{\epsilon}\cdot\boldsymbol{m}_n),$$

with $\hat{\epsilon}$ and $\hat{\epsilon}'$ the polarization state of the incident and diffracted x-ray beam, respectively. Note that, while f_m^1 scales with $\boldsymbol{m}$, f_m^2 scales with $\boldsymbol{m}^2$. Considering the extracted characteristic domain period, the magnetic diffracted intensity is mainly related to f_m^1. The diffracted intensity for a given incident beam polarization is expressed as follows [33]:

$$I(\boldsymbol{Q}) = \mathrm{Tr}[\tilde{f}_n\rho\tilde{f}_n^{\dagger}],$$

where $\tilde{f}_n$ and $\tilde{f}_n^{\dagger}$ are the Fourier transform of the scattering amplitude f_n and its complex conjugate, respectively, and ρ is the density matrix of the incident x-ray beam. In the Stoke-Poincaré representation [35], the density matrix for a circularly left or right incident beam is expressed as follows:

$$\rho_{\mathrm{CL}}=\begin{pmatrix}1 & -i\\ +i & 1\end{pmatrix},\qquad \rho_{\mathrm{CR}}=\begin{pmatrix}1 & +i\\ -i & 1\end{pmatrix}.$$

In the following, we consider two types of possible magnetic windings, i.e., helicoidal (or Bloch-like) and cycloidal (or Néel-like) depicted in Figs. 2(a) and 2(b), respectively, that are the ones expected in the multilayer systems considered here. From both these winding configurations, the magnetic asymmetry of their diffraction patterns can be calculated using $(I_{\mathrm{CL}}-I_{\mathrm{CR}})/(I_{\mathrm{CL}}+I_{\mathrm{CR}})$. In Fig. 2(c), we present the calculated orthoradial profiles of the normalized magnetic asymmetry for the two possible windings, and for each of them for the two possible chiralities, i.e., CW or CCW. For the case of a helicoidal winding (Bloch-like), the magnetic asymmetry is, respectively, maximum (for CW) and minimum (for CCW) in positions corresponding to an incident beam plane of $\psi=0$ or 180° and vanishes for $\psi=90°$ or 270°. On the contrary, for a cycloidal winding (Néel-like), the maximum (for CW) and minimum (for CCW) are obtained for $\psi=90°$ and 270°, respectively, resulting in the rotation of the dichroic diffraction pattern by 90° around the specular beam. Thus, it provides a simple way to determine unambiguously the actual texture of the domain wall from the orientation of the experimentally observed dichroism. Note that these calculations have been performed by taking into account only the magnetic part of the scattering amplitude, as in these unpatterned multilayers the anomalous charge scattering shall not result in any diffraction peak. In Fig. 2(d), we display the orthoradial experimental profile of the magnetic asymmetry we obtained for the $\|[\mathrm{Ir}(1)|\mathrm{Co}(0.8)|\mathrm{Pt}(1)]\times5$

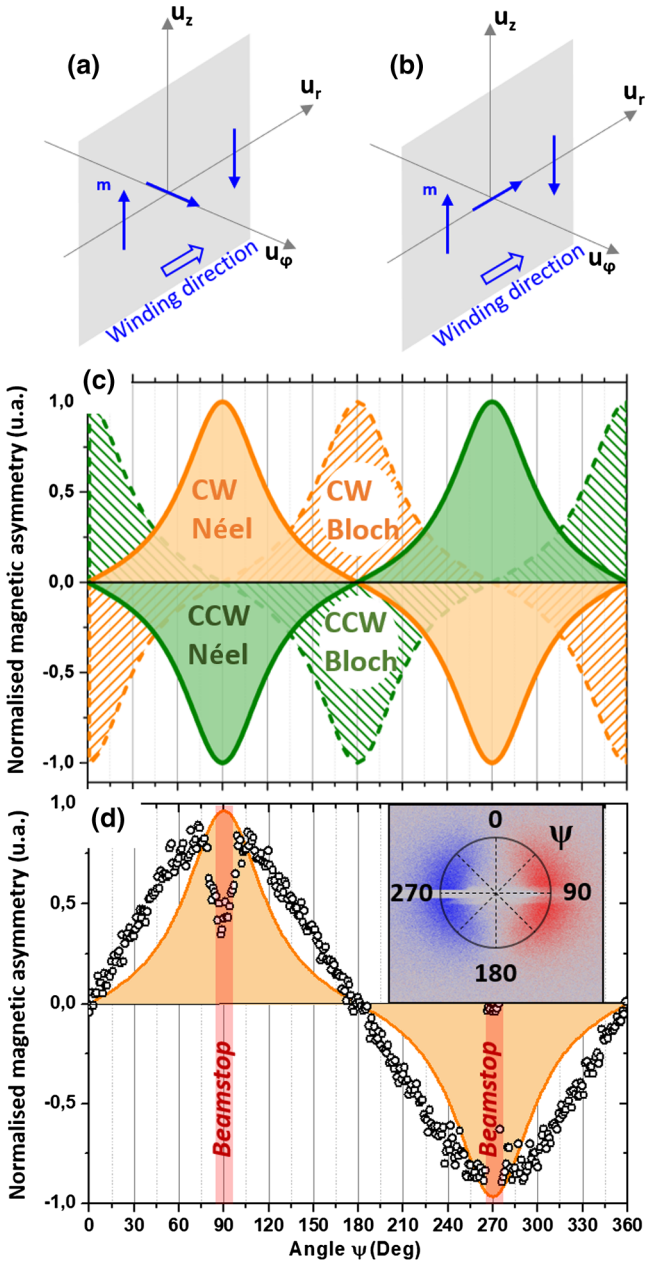

FIG. 2. (a) Diagram of a Bloch (helicoidal) winding and of a (b) Néel (cycloidal) winding. (c) Calculated orthoradial profile of the circular dichroism of different magnetic textures: CW (orange) and CCW (green) Bloch (dashed) and Néel (solid) windings for an incident angle $\theta = 17.5°$. (d) Comparison with the experimental magnetic asymmetry orthoradial profile of a $[\mathrm{Ir}(1)|\mathrm{Co}(0.8)|\mathrm{Pt}(1)] \times 5$ multilayer for the same incident angle $\theta = 17.5°$ (dots). Note that the red rectangles indicate the position of the beamstop.

multilayer measured at an incidence angle $\theta = 17.5°$. From the comparison with the predicted profile [yellow curve in Fig. 2(d)], and notably the positions of the maxima and minima, we can directly assert that the magnetic winding in our Ir|Co|Pt multilayers is of the Néel type. Hence, it confirms by a direct measurement and without assumptions that the DW texture is Néel (CW or CCW) as already known for this multilayer system with a significant interfacial DM interaction either indirectly through analysis of the Skyrmion size and comparison with micromagnetic simulations [27] or directly through Lorentz transmission electron microscopy [36]. From the sign of the magnetic asymmetry presented in Fig. 2(d), we conclude that the magnetic texture for sample $\|[\mathrm{Ir}(1)|\mathrm{Co}(0.8)|\mathrm{Pt}(1)] \times 5$ corresponds to a fixed CW Néel DW chirality. Finally, the global magnetic asymmetry pattern (changing sign only twice) allows us to corroborate that the overall topological winding number of the entire magnetic distribution is $N = 1$.

We notice that, beyond this qualitative comparison, a deviation between the measurement and the calculated curves in Fig. 2(d) outside the angles corresponding to the maxima and minima is present. We attribute it to the use of the kinematical approximation in our simulation that is known not to be strictly valid in the soft x-ray range [37] but, importantly, without affecting the main conclusion.

In order to experimentally confirm the origin of the dichroic contrast in the diffraction maps, we compare directly, in Fig. 3, two samples having the same multilayer constitution but opposite stacking: $\|[\mathrm{Ir}(1)|\mathrm{Co}(0.8)|\mathrm{Pt}(1)] \times 5$ (top of Fig. 3) or $\|[\mathrm{Pt}(1)|\mathrm{Co}(0.8)|\mathrm{Ir}(1)] \times 5$ (bottom of Fig. 3). In these two multilayers, a reversed direction of the DM vector is expected as predicted from the shape of the interfacial origin of the DM interaction [5,28] in bilayers or multilayers with magnetic material in contact with heavy materials. In Figs. 3(b) and 3(e), we display the MFM images obtained after demagnetization under a perpendicular field on each sample prior to the XRMS experiments. For both samples, a maze domain configuration is obtained, with a difference in the mean domain width [see the FFT in the insets in Figs. 3(b) and 3(e)] due to some (quasiunavoidable) non-negligible difference in the magnetic parameters of the two multilayers (perpendicular magnetic anisotropy, saturation magnetization, and DM interaction amplitude, etc.). However, despite these differences, it can be directly and unambiguously concluded from the dichroism XRMS diagram [Figs. 3(c) and 3(f)] that both the $\|\mathrm{Ir}|\mathrm{Co}|\mathrm{Pt}$ and $\|\mathrm{Pt}|\mathrm{Co}|\mathrm{Ir}$ multilayers have the same pure Néel domain wall configuration but with an opposite sense of rotation or winding sign. Indeed, they both present a complete disappearance of the dichroism for $\psi = 0$ or 180° but with a clear reversal of the sign of the dichroism. Thus, a simple XRMS map taking a few minutes (the dichroism is so large that even a single circular polarity might be enough to conclude) directly reveals that a system with Co on top of Pt has a CCW Néel DW configuration, while for Co below Pt, a CW Néel DW is found, as expected from theoretical predictions for bilayers. In order to corroborate our experimental conclusions, micromagnetic simulations have also been carried out. The result of energy minimization using

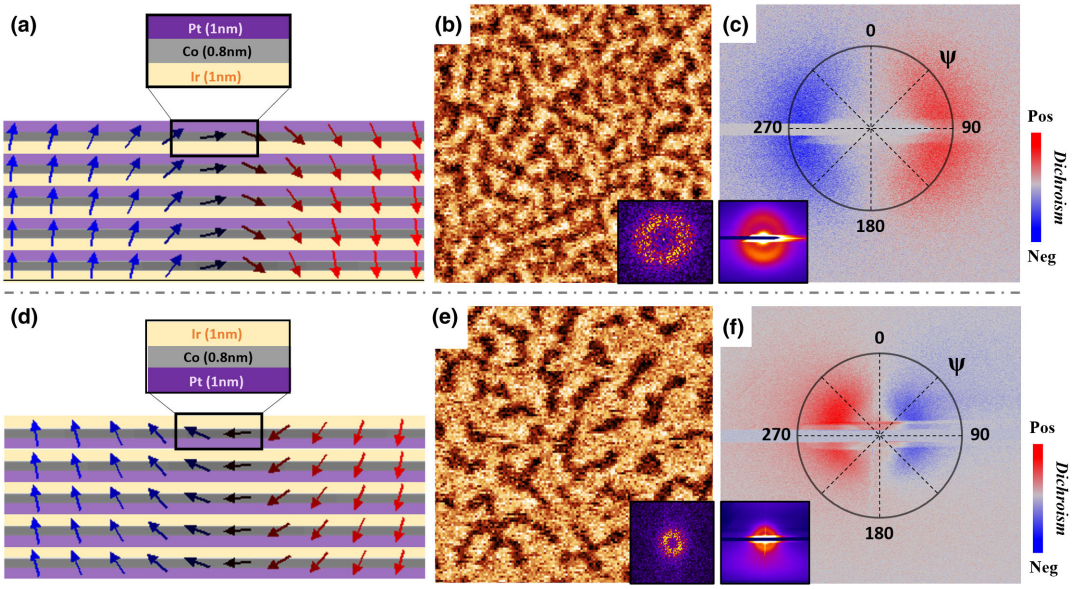

FIG. 3. Comparison of two samples with inverted stacking $\|[\mathrm{Ir}(1)|\mathrm{Co}(0.8)|\mathrm{Pt}(1)]\times 5$ (a)–(c) and $\|[\mathrm{Pt}(1)|\mathrm{Co}(0.8)|\mathrm{Ir}(1)]\times 5$ (d),(e). The corresponding magnetization textures are obtained by micromagnetic simulations based on material parameters (a),(d). (b),(e) MFM images with labyrinth-shape domains and their Fourier transform in the inset. (c),(f) Normalized magnetic asymmetry signal $(I_{\mathrm{CL}}-I_{\mathrm{CR}})/(I_{\mathrm{CL}}+I_{\mathrm{CR}})$ measured on sample a (e) and sample b (f). The diffraction sum images are shown in the inset, confirming again that the diffraction corresponds to the magnetic domains.

micromagnetic simulations using the MuMax3 code [38], using our film parameters, confirms that opposite Néel DW spin textures are expected in the two stackings [Figs. 3(a) and 3(d)]. A more detailed discussion about these micromagnetic simulations can be found elsewhere [39].

In conclusion, we investigated the magnetic asymmetry in x-ray resonant magnetic scattering to determine the chiral magnetic distribution, *i.e., its type (Néel or Bloch) and its magnetic chirality* in thin films presenting a strong DMI. In this work, we apply XRMS to the prototypical Pt|Co system, evidencing Néel-type domain walls as well as their chirality depending on the stacking order. This approach is fairly robust as the chirality due to domain walls as narrow as one-tenth of the domain width was easily accessed. This method can be applied to any type of magnetic materials, either in static or in time-resolved mode, and will be useful to investigate, for instance, metallic multilayers based on Co or Fe. Besides, further analysis associated with modeling might be performed to get some quantitative information such as the DM magnitude and even anisotropies. The power of this method is its unambiguous conclusion regarding the DMI sign independently of other magnetic parameters. In a broader perspective, magnetic asymmetry or circular dichroism in x-ray scattering appears to be a unique tool for studying the type and the chirality of the magnetic phase of any magnetic material. Similar investigations could be profitably extended to different types of systems showing a noncollinear magnetic ordering such as Skyrmion lattices or conical or helical phases stabilized by the Dzyaloshinskii-Moriya interaction as well as more complex systems such as the recently observed anti-Skyrmion lattices [40].

European Union Grant FLAG-ERA SoGraph (ANR-15-GRFL-0005) and MAGicSky (FET-634 Open-665095) are acknowledged for financial support.

*Corresponding author.
Jean-Yves.Chauleau@cea.fr
†Corresponding author.
vincent.cros@cnrs-thales.fr

[1] S. Heinze, K. von Bergmann, M. Menzel, J. Brede, A. Kubetzka, R. Wiesendanger, G. Bihlmayer, and S. Blügel, Nat. Phys. **7**, 713 (2011).
[2] I. Dzyaloshinsky, J. Phys. Chem. Solids **4**, 241 (1958).
[3] T. Moriya, Phys. Rev. **120**, 91 (1960).
[4] X. Z. Yu, Y. Onose, N. Kanazawa, J. H. Park, J. H. Han, Y. Matsui, N. Nagaosa, and Y. Tokura, Nature (London) **465**, 901 (2010).
[5] A. Fert, Mater. Sci. Forum **59–60**, 439 (1990).
[6] A. L. Balk, K.-W. Kim, D. T. Pierce, M. D. Stiles, J. Unguris, and S. M. Stavis, Phys. Rev. Lett. **119**, 077205 (2017).
[7] N. Romming, C. Hanneken, M. Menzel, J. E. Bickel, B. Wolter, K. von Bergmann, A. Kubetzka, and R. Wiesendanger, Science **341**, 636 (2013).
[8] J.-P. Tetienne, T. Hingant, L. J. Martínez, S. Rohart, A. Thiaville, L. H. Diez, K. Garcia, J.-P. Adam, J.-V. Kim, J.-F. Roch, I. M. Miron, G. Gaudin, L. Vila, B. Ocker, D. Ravelosona, and V. Jacques, Nat. Commun. **6**, 6733 (2015).

[9] Y. Dovzhenko, F. Casola, S. Schlotter, T. X. Zhou, F. Büttner, R. L. Walsworth, G. S. D. Beach, and A. Yacoby, arXiv:1611.00673.
[10] G. Chen, S. P. Kang, C. Ophus, A. T. N'Diaye, H. Y. Kwon, R. T. Qiu, C. Won, K. Liu, Y. Wu, and A. K. Schmid, Nat. Commun. **8**, 15302 (2017).
[11] S. D. Pollard, J. A. Garlow, J. Yu, Z. Wang, U. Zhu, and H. Yang, Nat. Commun. **8**, 14761 (2017).
[12] M. Belmeguenai, J.-P. Adam, Y. Roussigné, S. Eimer, T. Devolder, J.-V. Kim, S. M. Cherif, A. Stashkevich, and A. Thiaville, Phys. Rev. B **91**, 180405(R) (2015).
[13] H. S. Körner, J. Stigloher, H. G. Bauer, H. Hata, T. Taniguchi, T. Moriyama, T. Ono, and C. H. Back, Phys. Rev. B **92**, 220413(R) (2015).
[14] M. Blume and O. C. Kistner, Phys. Rev. **171**, 417 (1968).
[15] H. A. Dürr, E. Dudzik, S. S. Dhesi, J. B. Goedkoop, G. Van der Laan, M. Belakhovsky, C. Mocuta, A. Marty, and Y. Samson, Science **284**, 2166 (1999).
[16] S. S. P. Parkin and S. H. Yang, Nat. Nanotechnol. **10**, 195 (2015).
[17] A. Fert, V. Cros, and J. Sampaio, Nat. Nanotechnol. **8**, 152 (2013).
[18] A. V. Khvalkovskiy, V. Cros, D. Apalkov, V. Nikitin, M. Krounbi, K. A. Zvezdin, A. Anane, J. Grollier, and A. Fert, Phys. Rev. B **87**, 020402 (2013).
[19] A. Thiaville, S. Rohart, É. Jué, V. Cros, and A. Fert, Europhys. Lett. **100**, 57002 (2012).
[20] J. Torrejon, J. Kim, J. Sinha, S. Mitani, M. Hayashi, M. Yamanouchi, and H. Ohno, Nat. Commun. **5**, 4655 (2014).
[21] P.-H. Jang, K. Song, S.-J. Lee, S.-W. Lee, and K.-J. Lee, Appl. Phys. Lett. **107**, 202401 (2015).
[22] J. Sampaio, A. V. Khvalkovskiy, M. Kuteifan, M. Cubukcu, D. Apalkov, V. Lomakin, V. Cros, and N. Reyren, Appl. Phys. Lett. **108**, 112403 (2016).
[23] E. Jal, V. López-Flores, N. Pontius, T. Ferté, N. Bergeard, C. Boeglin, B. Vodungbo, J. Lüning, and N. Jaouen, Phys. Rev. B **95**, 184422 (2017).
[24] B. Pfau, S. Schaffert, L. Müller, C. Gutt, A. Al-Shemmary, F. Büttner, R. Delaunay, S. Düsterer, S. Flewett, R. Frömter, J. Geilhufe, E. Guehrs, C. M. Günther, R. Hawaldar, M. Hille, N. Jaouen, A. Kobs, K. Li, J. Mohanty, H. Redlin, W. F. Schlotter, D. Stickler, R. Treusch, B. Vodungbo, M. Kläui, H. P. Oepen, J. Lüning, G. Grübel, and S. Eisebitt, Nat. Commun. **3**, 1100 (2012).
[25] I. M. Miron, G. Gaudin, S. Auffret, B. Rodmacq, A. Schuhl, S. Pizzini, J. Vogel, and P. Gambardella, Nat. Mater. **9**, 230 (2010).
[26] L. Liu, C.-F. Pai, Y. Li, H. W. Tseng, D. C. Ralph, and R. A. Buhrman, Science **336**, 555 (2012).
[27] C. Moreau-Luchaire, C. Moutafis, N. Reyren, J. Sampaio, C. A. F. Vaz, N. Van Horne, K. Bouzehouane, K. Garcia, C. Deranlot, P. Warnicke, P. Wohlhüter, J.-M. George, M. Weigand, J. Raabe, V. Cros, and A. Fert, Nat. Nanotechnol. **11**, 444 (2016).
[28] H. Yang, A. Thiaville, S. Rohart, A. Fert, and M. Chshiev, Phys. Rev. Lett. **115**, 267210 (2015).
[29] M. Sacchi, N. Jaouen, H. Popescu, R. Gaudemer, J. M. Tonnerre, S. G. Chiuzbaian, C. F. Hague, A. Delmotte, J. M. Dubuisson, G. Cauchon, B. Lagarde, and F. Polack, J. Phys. Conf. Ser. **425**, 0720182013).
[30] N. Jaouen, J.-M. Tonnerre, G. Kapoujian, P. Taunier, J.-P. Roux, D. Raoux, and F. Sirotti, J. Synchrotron Radiat. **11**, 353 (2004).
[31] S. L. Zhang, G. van der Laan, and T. Hesjedal, Nat. Commun. **8**, 14619 (2017).
[32] A. Fert, N. Reyren, and V. Cros, Nat. Rev. Mater. **2**, 17031 (2017).
[33] J. P. Hannon, G. T. Trammell, M. Blume, and D. Gibbs, Phys. Rev. Lett. **61**, 1245 (1988).
[34] J. P. Hill and D. F. McMorrow, Acta Crystallogr. Sect. A **52**, 236 (1996).
[35] G. van der Laan, C.R. Phys. **9**, 570 (2008).
[36] J. F. Pulecio, A. Hrabec, K. Zeissler, R. M. White, Y. Zhu, and C. H. Marrows, arXiv:1611.06869.
[37] A. Authier, in *Reciprocal Space*, International Tables for Crystallography Vol. B (Springer, New York, 2006), pp. 534–551.
[38] A. Vansteenkiste, J. Leliaert, M. Dvornik, M. Helsen, F. Garcia-Sanchez, and B. Van Waeyenberge, AIP Adv. **4**, 107133 (2014).
[39] W. Legrand, J.Y Chauleau, D. Maccariello, N. Reyren, S. Collin, K. Bouzehouane, N. Jaouen, V. Cros, and A. Fert, arXiv:1712.05978.
[40] A. K. Nayak, V. Kumar, T. Ma, P. Werner, E. Pippel, R. Sahoo, F. Damay, U. K. Rößler, C. Felser, and S. S. P. Parkin, Nature (London) **548**, 561 (2017).